DOI: 10.1002/adma.200801056

Multicolor Core/Shell-Structured Upconversion Fluorescent Nanoparticles**

By *Zhengquan Li, Yong Zhang,** and *Shan Jiang*

Near-infrared (NIR)-to-Visible upconversion fluorescent nanoparticles emit visible light upon NIR-light excitation, and are well suited for bioimaging, compared to the commonly used downconversion fluorescent materials. These nanoparticles have advantages such as minimum photodamage to living organisms, weak background fluorescence, high detection sensitivity, and high light-penetration depth in tissues. However, development of upconversion fluorescent nanoparticles is still in its infancy, and such materials have yet to be used for bioimaging applications due to their unsuitable surface properties, poor dispersibility in water, and limited colors. In this work, facile and user-friendly methods are developed to synthesize uniform $NaYF_4$ nanospheres with strong upconversion fluorescence and core–shell silica/$NaYF_4$ nanospheres with uniform silica coating on the surface. Multicolor upconversion nanospheres are produced by encapsulating organic dyes or quantum dots (QDs) in the silica shell, and upconversion fluorescence is generated based on fluorescence resonance energy transfer (FRET) from the $NaYF_4$ nanospheres to these organic dyes or QDs. Use of the upconversion nanospheres for imaging of cells is also demonstrated, the first report in the field using such nanoparticles for bioimaging.

Fluorescence imaging is a very important technique for biological studies and clinical applications. It has been used for in vivo imaging due to its high temporal and spatial resolutions.[1] Conventional fluorescence imaging is based on single-photon excitation, emitting low-energy fluorescence when excited by a high-energy light. It has some limitations, such as causing DNA damage and cell death due to long-term irradiation with UV or short-wavelength light, significant auto-fluorescence from biological tissues, resulting in low signal-to-noise ratios, and short penetration depth of short-wavelength excitation light in biological tissues.[2] Two-photon fluorescence imaging (TPFI) is a novel technique that generates high-energy visible photons from low-energy radiation in NIR region.[3] NIR radiation is less harmful to cells, minimizes auto-fluorescence from biological tissues, and penetrates tissues to a greater extent.[4] So far, most commercially available two-photon fluorophores are organic dyes that exhibit relatively low two-photon absorption cross-sections, low fluorescence quantum yield, and photochemical instability (photobleaching). Some efforts have been made to prepare better organic fluorophores with tailored properties.[5] Some inorganic materials, such as semiconductor quantum dots (QDs) and metal nanospheres or nanorods, have also been developed and used for two-photon imaging of cells.[6–9] However, TPFI requires nearly simultaneous absorption of two coherent NIR photons, and therefore, the efficiency is usually low, and expensive pulsed lasers are usually required. Photon upconversion is an alternative process for converting NIR radiation to visible radiation. It is based on sequential (not simultaneous) absorption of photons, and as such its efficiency is much higher compared to two-photon absorption, and continuous wave (CW) lasers can be used for excitation. Typical laser power densities are 1–10^3 W cm^{-2} for upconversion and 10^6–10^9 W cm^{-2} for two-photon absorption. Pulsed lasers are normally used for downconversion fluorescent materials. Although the average power density is on the order of 50–400 mW cm^{-2}, the peak power density could be quite high. Upconversion fluorescent materials can be excited by CW lasers. Biological cells and tissues have very weak absorption in the NIR region, and as such increasing the laser power does not cause any significant heat damage.

Various inorganic crystals doped with lanthanide ions have been synthesized, producing strong NIR-to-vis upconversion fluorescence. These are very promising materials for bioimaging, because the rare-earth elements used in their synthesis have lower toxicity than the semiconductor elements of QDs (LD_{50} is approximately a thousand times higher than that of QDs), while the upconversion fluorescence is much stronger than that of QDs.[10–12] These materials have been used in immunohistochemistry in lateral flow (LF) assay formats, and in immunochromatographic assays of human chorionic gonadotropin (hCG).[13–17] Hosting of in vitro nucleic acid assays has also been described.[18,19] Furthermore, 150 nm sized particles have been inoculated into live *Caenorhabditis elegans,* and imaged in the intestines of the worms; however, no biological materials were used for the particle surface

[*] Prof. Y. Zhang, S. Jiang
Division of Bioengineering
National University of Singapore
Singapore 117574 (Singapore)
E-mail: biezy@nus.edu.sg
Prof. Y. Zhang
Nanoscience and Nanotechnology Initiative
National University of Singapore
Singapore 117576 (Singapore)
Dr. Z. Li
Singapore-MIT Alliance
National University of Singapore
4 Engineering Drive 3, Singapore 117576 (Singapore)

[**] The authors would like to acknowledge the financial support from Singapore A*STAR BMRC (grant number R-397-000-624-305) and from the National University of Singapore, and Z. Li acknowledges support from the Singapore-Massachusetts Institute of Technology Alliance (SMA). Supporting Information is available online from Wiley InterScience or from the author.

ADVANCED MATERIALS

functionalization, and the particles were taken up by the worms from the nutrient media through the digestive tract.[20] These particles are not suitable for imaging of cells and animals because of their large sizes and nonfunctionalized surfaces.

Among these lanthanide-doped materials, Yb/Er (or Yb/Tm) codoped $NaYF_4$ nanoparticles have been reported as the most efficient NIR-to-vis upconversion fluorescent material,[21] and show strong upconversion fluorescence, seven orders of magnitude higher than that of CdSe–ZnS QDs.[11,12] These nanoparticles are usually synthesized in organic solvents or at high temperatures.[22–24] Ethylenediamine tetraacetic acid (EDTA) has been used as a chelating agent to control the growth of $NaYF_4$ nanocrystals, and thermal decomposition of mixed trifluoroacetates has been used to produce high-quality cubic- and hexagonal-phase $NaYF_4$ nanocrystals.[11,24–26] However, these nanocrystals can be dispersed only in some organic solvents to form colloidal solutions after sonication, but not in water. Very recently, we reported a method using poly(vinyl pyrrolidone) (PVP) as a chelating agent and surfactant to control the size and stability of the nanocrystals, rendering them dispersible in some commonly used organic solvents and water. Nevertheless, the surfactant used does not lend itself to easy modification with biomolecules, and further surface modification of the nanocrystals is still required.[27] Coating of the nanoparticles with a layer of silica is preferred, but forming silica coatings directly on hydrophobic nanoparticles is arduous. Furthermore, producing uniform and thin silica shells on individual nanoparticles rather than on particle aggregates is quite challenging.

In this work, uniform hexagonal-phase $NaYF_4$ nanospheres with strong upconversion fluorescence and core/shell silica/$NaYF_4$ structures are produced, with uniform silica coating on the surface. Multicolor spheres are produced by encapsulating organic dyes or QDs into the silica shell, and upconversion fluorescence is generated based on FRET from the $NaYF_4$ cores to organic dyes or QDs.

Oleic acid was used as the surfactant, to control the size and shape of the $NaYF_4$:Yb,Er/Tm nanocrystals, which showed different shapes when the concentration of oleic acid was changed. Transmission electron microscopy (TEM) images of the nanocrystals in Figure 1a and b showed that when

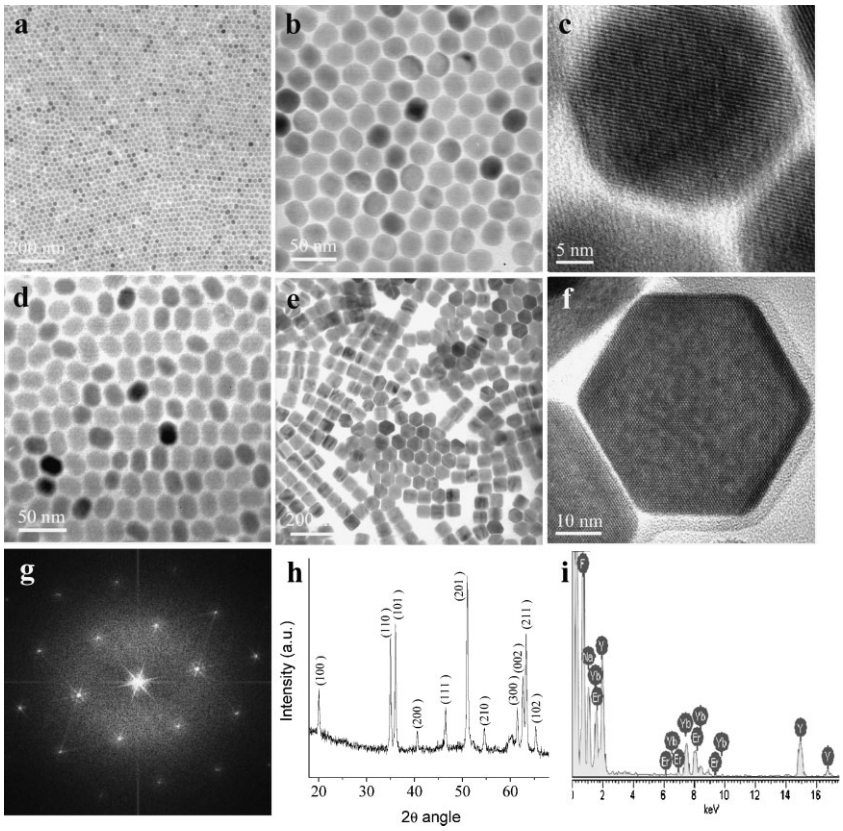

Figure 1. Control of nanocrystal shape. a–c) TEM images of $NaYF_4$:Yb,Er nanospheres at different magnifications. d) TEM images of $NaYF_4$:Yb,Er nanoellipses. e,f) TEM images of $NaYF_4$:Yb,Er nanoplates at different magnifications. g) Fourier Transform of TEM image in f). h) XRD pattern and i) EDAX analysis of $NaYF_4$:Yb,Er nanospheres.

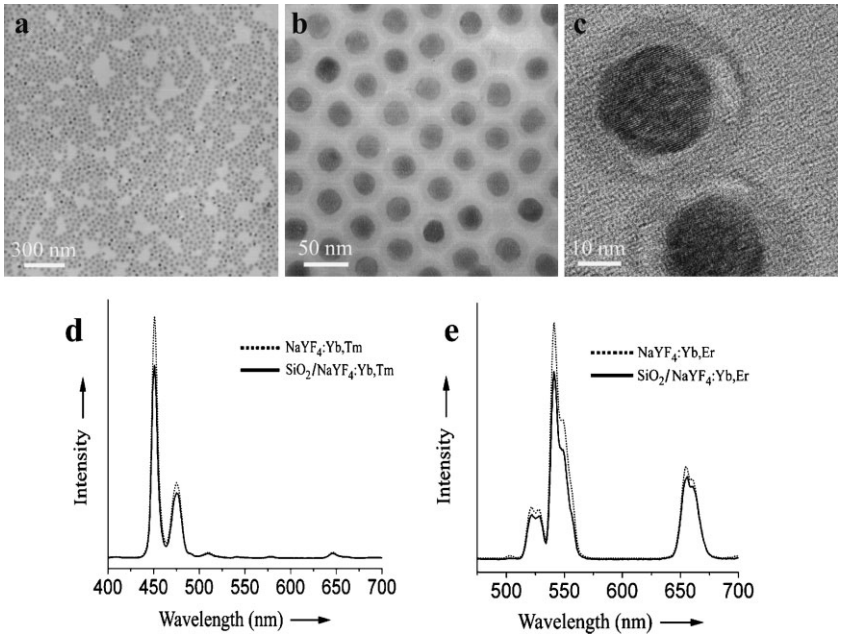

Figure 2. Coating of silica on nanocrystals. a–c) TEM images of silica-coated $NaYF_4$:Yb,Er nanospheres at different magnifications and fluorescence spectra of d) $NaYF_4$:Yb,Tm e) and $NaYF_4$:Yb,Er nanospheres, with and without silica coating.

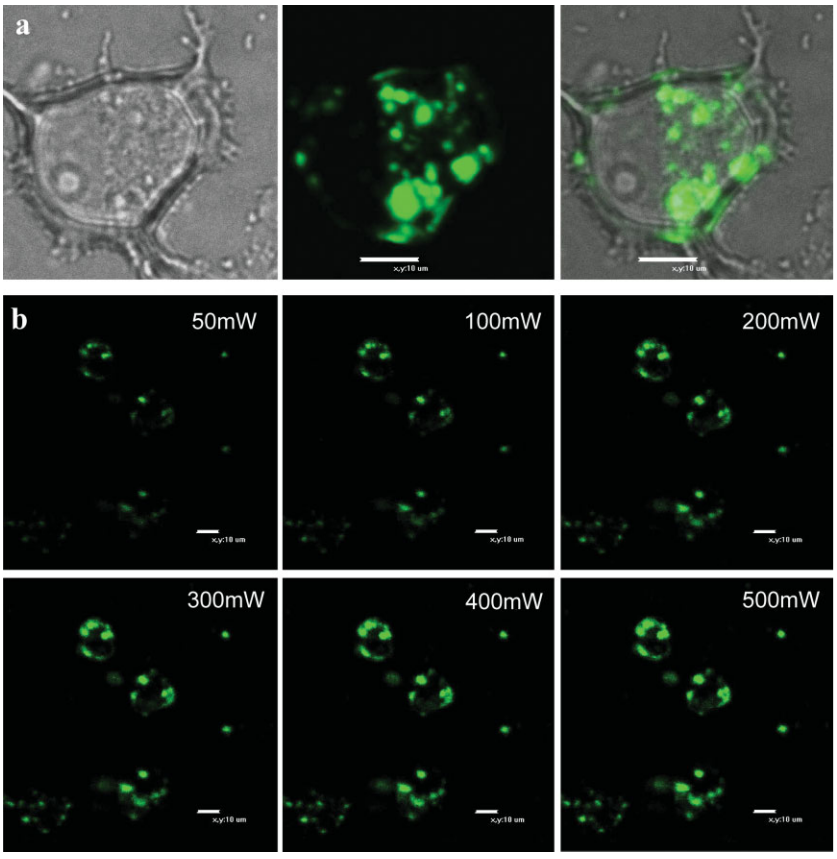

Figure 3. Confocal fluorescence imaging of MCF-7 cells using silica/$NaYF_4$:Yb,Er nanospheres. a) Bright-field (left), confocal fluorescence (middle), and superimposed (right) images of MCF-7 cells incubated with the nanospheres for 24 h. b) Confocal fluorescence images of MCF-7 cells with the nanospheres, excited by a 980 nm laser with different power intensities.

6 mL oleic acid was added to the precursor solution, the nanocrytals were polyhedral in shape (nanospheres), with a uniform size of (21 ± 0.5) nm in diameter. The nanospheres were easily self-assembled on the carbon grid, in a long-range order. The crystal lattice, with an interplanar distance of 5.2 Å, is shown in the high-resolution TEM image in Figure 1c, corresponding to the (100) plane of the nanocrystals. When 10 mL oleic acid was added to the precursor solution, elliptical nanocrystals with a width of 17 nm and a length of 22 nm were obtained, as shown in Figure 1d. With the amount of oleic acid decreased to 3 mL, uniform hexagonal plate-like $NaYF_4$:Yb,Er/Tm nanocrystals (nanoplates) were produced, as shown in Figure 1e. The nanoplate has a flat hexagonal top surface, with an edge length of ~30 nm and six rectangular side surfaces with a surface area of $\sim 30\,\text{nm} \times 45\,\text{nm}$. The crystal lattice of the nanoplate is shown in the high-resolution TEM image in Figure 1f, indicating high crystallinity. The Fourier transform of the TEM image of a single nanoplate (Figure 1g) further demonstrates the perfect hexagonal crystal structure and uniformity of the nanoplates. The X-ray diffraction (XRD) pattern and energy-dispersive X-ray analysis (EDXA) results for the hexagonal-phase $NaYF_4$:Yb,Er nanocrystals are also displayed in Figure 1. All diffraction peaks could be indexed to pure hexagonal-phase $NaYF_4$ crystals (JCPDS standard card no. 28-1192). No diffraction peaks corresponding to cubic-phase crystals or other impurities were observed. The presence of Yb and Er in the nanocrystals was confirmed by the EDXA result, and the amount of Y, Yb, and Er were quantified using inductively coupled plasma – atomic emission spectrometry (ICP-AES), and the Y/Yb/Er molar ratio were determined to be 79.2:18.6:2.2, which is the stoichiometric ratio for the chloride reactants used in the experiment.

The most commonly used methods for coating silica on nanocrystals are the Stober method and the microemulsion method. The Stober method is usually used for nanocrystals that can be well dispersed in polar solvents such as ethanol and isopropanol, and as such is not suitable for hydrophobic nanocrystals.[28] The microemulsion method has been used for coating silica on hydrophobic nanocrystals such as QDs and Fe_3O_4 nanoparticles. However, coating individual nanoparticles with very thin shells is quite challenging.[29,30] To coat hydrophobic $NaYF_4$ nanocrystals, these were first dispersed in cyclohexane, and then surfactants and ammonia were added to form a water-in-oil microemulsion. A relatively high nanocrystal concentration was used, and the emulsion was sonicated to ensure single nanocrystals were encapsulated in each microemulsion pool. It was found that such a method was very efficient for fabricating thin and uniform silica shells. The TEM images in Figure 2a–c show that this method can be used for large-scale synthesis of core/shell-structured $NaYF_4$ nanocrystals with thin, uniform silica coatings on the surface. The thickness of the silica shell was about (8 ± 1.5) nm, much smaller than the diameter of the nanocrystal. After silica coating, the nanocrystals were dispersible in water with good chemical and photochemical stability (Supporting Information), and a clear colloidal solution was formed. Furthermore, biomolecules were conjugated to the silica surface using well-established protocols. Fluorescence spectra of transparent colloidal solutions of $NaYF_4$:Yb,Er/Tm nanospheres in hexane (0.01 M) and silica/$NaYF_4$:Yb,Er/Tm nanospheres in water (0.01 M) are shown in Figure 2d and e. The emission peaks of $NaYF_4$:Yb,Er nanospheres at 407, 521, 539, and 651 nm were due to the transitions from the energy levels $^4H_{9/2}$, $^4H_{11/2}$, $^4S_{3/2}$, and $^4F_{9/2}$ to $^4I_{15/2}$ of Er^{3+}. Two emission peaks of $NaYF_4$:Yb,Tm nanospheres, at 450 and 479 nm, were due to $^1D_2 \rightarrow {}^3F_4$ and $^1G_4 \rightarrow {}^3H_6$ transitions of Tm^{3+}.[31] The silica-coated nanospheres showed a small decrease in fluorescence intensity compared to the uncoated nanospheres.

ADVANCED MATERIALS

Silica/$NaYF_4$:Yb,Er nanospheres were incubated in physiological conditions with MCF-7 cells for 24 h. The unbound nanospheres were washed away, and the live cells were imaged in bright field and with NIR excitation using a confocal microscope equipped with a 980 nm NIR laser (Fig. 3a). Fluorescence from the nanospheres was observed in the cells with high signal-to-background ratio, while the control cells, incubated without the nanospheres, showed no fluorescence under similar imaging parameters and conditions. Due to the unique optical properties of upconversion nanospheres (very low autofluorescence from biological cells under excitation of 980 nm laser), increase in the output power of the laser increases the fluorescence signal from the nanospheres but not the noise (Fig. 3b).

$NaYF_4$ nanocrystals with different-color upconversion fluorescences can be obtained by doping various upconverting lanthanide ions into the nanocrystals. So far, only nanocrystals codoped with Yb/Er or Yb/Tm have been produced, which emit green or blue fluorescence with sufficiently high upconversion efficiencies. The Yb ions absorb NIR light, followed by energy transfer to the Er/Tm ions, which emit visible light. Although the emitter can be excited directly, codoping of the absorber, such as Yb ions, in the nanocrystals usually generates stronger upconversion fluorescence, because these ions have a broad and strong absorption at ~980 nm (the absorption cross-section of Yb is ten times larger than that of Er/Tm). However, the nanocrystals are not suitable for multiplexing biodetection, due to their limited number of colors. It is necessary to develop upconversion nanoparticles with multicolor fluorescence emission under NIR excitation at the same wavelength. Our strategy is to prepare core/shell-structured nanospheres with the upconversion nanocyrstals as the core and multicolor downconversion materials, such as fluorescent dyes or QDs, doped into the shell. The upconversion nanocrystals are used as energy donors, and the downconversion materials are used as energy acceptors. The upconversion nanocrystals (the core) absorb NIR radiation at a single wavelength, and the emitted visible fluorescence is then absorbed by the downconversion materials (in the shell) that emit multicolor fluorescence, as shown in Figure 4a. Two commonly used fluorescent dyes, fluorescein isothiocyanate (FITC) and tetramethylrhodamine isothiocyanate (TRITC), and QDs (QD605) were encapsulated into the silica shell of silica/$NaYF_4$:Yb,Er/Tm nanospheres, and used as examples to prove the concept. The dyes were first grafted to (3-aminopropyl)triethoxysilane (APS) to improve their stability, and then the mixture was cohydrolyzed with TEOS to form the silica coatings on the upconversion nanospheres using the microemulsion method. The morphologies of FITC-doped silica/$NaYF_4$:Yb,Tm nanospheres, TRITC-doped silica/$NaYF_4$:Yb,Er nanospheres, and

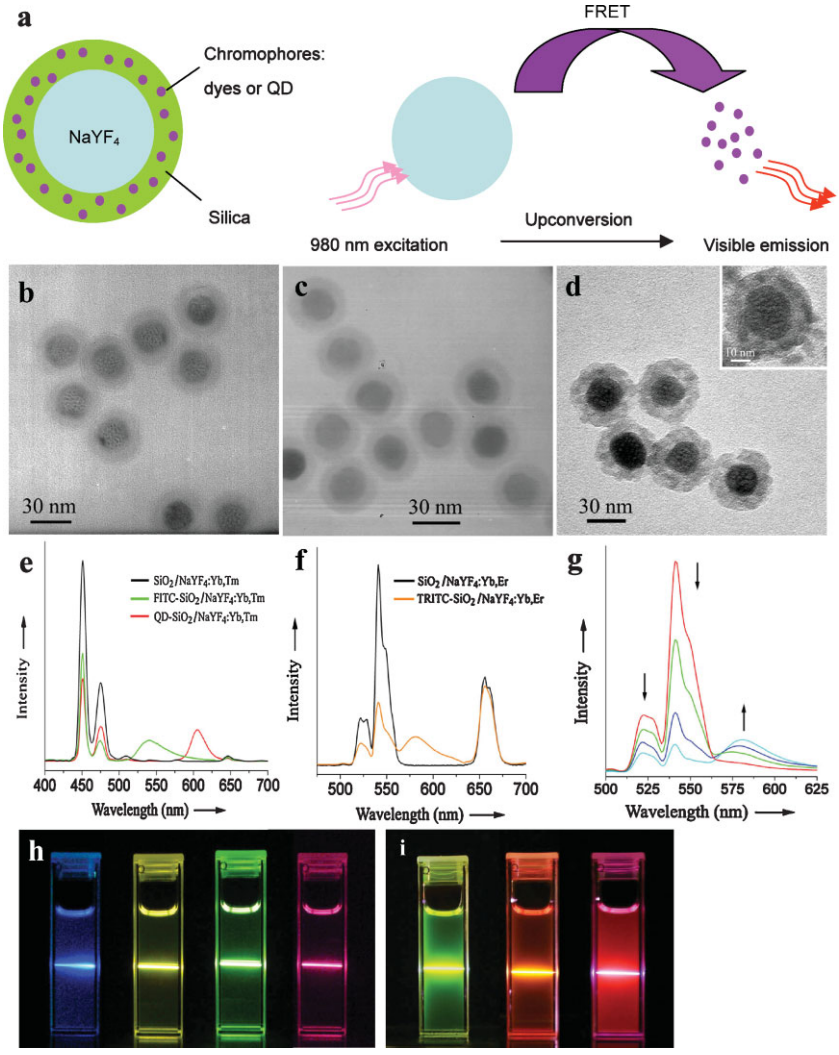

Figure 4. Multicolor NIR-to-vis upconversion nanospheres. a) Schematic drawing of FRET-based multicolor silica/$NaYF_4$ NIR-to-vis upconversion nanospheres. TEM images of b) FITC-doped silica/$NaYF_4$:Yb,Tm nanospheres, c) TRITC-doped silica/$NaYF_4$:Yb,Er nanospheres, and d) QD605-doped silica/$NaYF_4$:Yb,Tm nanospheres. e) Fluorescence spectra of pure silica/$NaYF_4$:Yb,Tm nanospheres (black line) and of nanospheres doped with FITC (green line) and QD605 (red line). f) Fluorescence spectra of pure silica/$NaYF_4$:Yb,Er nanospheres (black line) and of nanospheres doped with TRITC (red line). g) Fluorescence spectra of silica/$NaYF_4$:Yb, Er nanospheres (0.01 mmol) doped with different amounts of TRITC (10, 20, 30, and 40 nmol). h) Photographs of silica/$NaYF_4$ nanospheres in hexane (1 wt %) under excitation of NIR laser (980 nm, power density = 50 W cm^{-2}): total upconversion fluorescence of $NaYF_4$:Yb,Tm nanospheres (blue), total upconversion fluorescence of $NaYF_4$:Yb,Er nanospheres (yellow green), and fluorescence passing through red (green) or green (red) filters. i) Photographs showing total fluorescence of FITC-doped silica/$NaYF_4$:Yb,Tm nanospheres (left), TRITC-doped silica/$NaYF_4$:Yb,Er nanospheres (middle), and QD605-doped silica/$NaYF_4$:Yb,Tm nanospheres (right).

QD605-doped silica/$NaYF_4$:Yb,Tm nanospheres are shown in Figure 4b–d, and are similar to that of the undoped nanospheres. The high-resolution TEM image in Figure 4d demonstrates the presence of QDs in the silica shell. The fluorescence spectra of FITC- and QD605-doped silica/$NaYF_4$:Yb,Tm nanospheres are given in Figure 4e. The characteristic emission peaks of undoped silica/$NaYF_4$:Yb,Tm nanospheres at 450 and 479 nm were reduced, while new emission peaks, of FITC and QD605 at 536 and 605 nm, respectively, appeared, suggesting an efficient FRET between the nanocrystals and dyes (QD605).

Similar phenomena were observed for TRITC-doped silica/$NaYF_4$:Yb,Er nanospheres, as shown in Figure 4f. The red emission peak at 651 nm was unchanged, because the fluorescence emitted at this wavelength was not absorbed by TRITC. The spectra of silica/$NaYF_4$:Yb,Er nanospheres doped with different amounts of TRITC are given in Figure 4g. The fluorescence intensity is proportional to the amount of TRITC used. Strong fluorescence with different colors from silica/$NaYF_4$:Yb,Er/Tm nanospheres and the nanospheres doped with FITC, TRITC, and QD605 was observed under excitation with a 980 nm NIR laser, and the photographs are given in Figure 4h and i. The fluorescence could still be observed when the power density of the laser was reduced to 1 $W\,cm^{-2}$. The strong fluorescence is probably due to the high crystallinity and uniformity of the nanocrystals.

In conclusion, core/shell-structured pure-hexagonal-phase $NaYF_4$:Yb,Er/Tm nanospheres with very thin and uniform silica coatings are prepared. The nanospheres emit strong NIR-to-vis upconversion fluorescence, and are used as fluorescent probes in cell imaging. Multicolor upconversion fluorescent nanospheres are produced by encapsulating organic dyes or QDs into the silica shell, and upconversion fluorescence is generated based on FRET from the $NaYF_4$ core to the organic dyes or QDs. These materials will be very useful for in vitro multiplexed bioassays and in vivo studies.

Experimental

Detailed experimental procedures are reported in the Supporting Information.

Received: April 16, 2008
Revised: August 6, 2008
Published online: October 20, 2008

[1] J. H. Rao, A. Dragulescu-Andrasi, H. Q. Yao, H. Q. Yao, *Curr. Opin. Biotechnol.* **2007**, *18*, 17.
[2] Q. L. de Chermont, C. Chaneac, J. Seguin, F. Pelle, S. Maitrejean, J. P. Jolivet, D. Gourier, M. Bessodes, D. Scherman, *Proc. Natl. Acad. Sci. USA* **2007**, *104*, 9266.
[3] K. Schenke-Layland, I. Riemann, O. Damour, U. A. Stock, K. Konig, *Adv. Drug Delivery Rev.* **2006**, *58*, 878.
[4] J. V. Frangioni, *Curr. Opin. Chem. Biol.* **2003**, *7*, 626.
[5] M. Oheim, D. J. Michael, M. Geisbauer, D. Madsen, R. H. Chow, *Adv. Drug Delivery Rev.* **2006**, *58*, 788.
[6] N. J. Durr, T. Larson, D. K. Smith, B. A. Korgel, K. Sokolov, A. Ben-Yakar, *Nano Lett.* **2007**, *7*, 941.
[7] K. T. Yong, J. Qian, I. Roy, H. H. Lee, E. J. Bergey, K. M. Tramposch, S. L. He, M. T. Swihart, A. Maitra, P. N. Prasad, *Nano Lett.* **2007**, *7*, 761.
[8] X. F. Yu, L. D. Chen, Y. L. Deng, K. Y. Li, Q. Q. Wang, Y. Li, S. Xiao, L. Zhou, X. Luo, J. Liu, D. W. Pang, *J. Fluoresc.* **2007**, *17*, 243.
[9] H. F. Wang, T. B. Huff, D. A. Zweifel, W. He, P. S. Low, A. Wei, J. X. Cheng, *Proc. Natl. Acad. Sci. USA* **2005**, *102*, 15752.
[10] R. J. Palmer, J. L. Butenhoff, J. B. Stevens, *Environ. Res.* **1987**, *43*, 142.
[11] S. Heer, K. Kompe, H. U. Gudel, M. Haase, *Adv. Mater.* **2004**, *16*, 2102.
[12] D. R. Larson, W. R. Zipfel, R. M. Williams, S. W. Clark, M. P. Bruchez, F. W. Wise, W. W. Webb, *Science* **2003**, *300*, 1434.
[13] P. Corstjens, M. Zuiderwijk, A. Brink, S. Li, H. Feindt, R. S. Neidbala, H. Tanke, *Clin. Chem.* **2001**, *47*, 1885.
[14] P. Corstjens, M. Zuiderwijk, M. Nilsson, H. Feindt, R. S. Niedbala, H. J. Tanke, *Anal. Biochem.* **2003**, *312*, 191.
[15] J. Hampl, M. Hall, N. A. Mufti, Y. M. M. Yao, D. B. MacQueen, W. H. Wright, D. E. Cooper, *Anal. Biochem.* **2001**, *288*, 176.
[16] R. S. Niedbala, H. Feindt, K. Kardos, T. Vail, J. Burton, B. Bielska, S. Li, D. Milunic, P. Bourdelle, R. Vallejo, *Anal. Biochem.* **2001**, *293*, 22.
[17] H. Zijlmans, J. Bonnet, J. Burton, K. Kardos, T. Vail, R. S. Niedbala, H. J. Tanke, *Anal. Biochem.* **1999**, *267*, 30.
[18] F. van de Rijke, H. Zijlmans, S. Li, T. Vail, A. K. Raap, R. S. Niedbala, H. J. Tanke, *Nat. Biotechnol.* **2001**, *19*, 273.
[19] P. Zhang, S. Rogelj, K. Nguyen, D. Wheeler, *J. Am. Chem. Soc.* **2006**, *128*, 12410.
[20] S. F. Lim, R. Riehn, W. S. Ryu, N. Khanarian, C. K. Tung, D. Tank, R. H. Austin, *Nano Lett.* **2006**, *6*, 169.
[21] K. W. Kramer, D. Biner, G. Frei, H. U. Gudel, M. P. Hehlen, S. R. Luthi, *Chem. Mater.* **2004**, *16*, 1244.
[22] S. Heer, O. Lehmann, M. Haase, H. U. Gudel, *Angew. Chem. Int. Ed.* **2003**, *42*, 3179.
[23] G. S. Yi, B. Q. Sun, F. Z. Yang, D. P. Chen, Y. X. Zhou, J. Cheng, *Chem. Mater.* **2002**, *14*, 2910.
[24] J. H. Zeng, J. Su, Z. H. Li, R. X. Yan, Y. D. Li, *Adv. Mater.* **2005**, *17*, 2119.
[25] J. C. Boyer, F. Vetrone, L. A. Cuccia, J. A. Capobianco, *J. Am. Chem. Soc.* **2006**, *128*, 7444.
[26] G. S. Yi, H. C. Lu, S. Y. Zhao, G. Yue, W. J. Yang, D. P. Chen, L. H. Guo, *Nano Lett.* **2004**, *4*, 2191.
[27] Z. Q. Li, Y. Zhang, *Angew. Chem. Int. Ed.* **2006**, *45*, 7732.
[28] C. Graf, D. L. J. Vossen, A. Imhof, A. van Blaaderen, *Langmuir* **2003**, *19*, 6693.
[29] M. Darbandi, R. Thomann, T. Nann, *Chem. Mater.* **2005**, *17*, 5720.
[30] D. K. Yi, S. T. Selvan, S. S. Lee, G. C. Papaefthymiou, D. Kundaliya, J. Y. Ying, *J. Am. Chem. Soc.* **2005**, *127*, 4990.
[31] J. F. Suyver, A. Aebischer, D. Biner, P. Gerner, J. Grimm, S. Heer, K. W. Kramer, C. Reinhard, H. U. Gudel, *Opt. Mater.* **2005**, *27*, 1111.